Research Square

Preprints are preliminary reports that have not undergone peer review.
They should not be considered conclusive, used to inform clinical practice,
or referenced by the media as validated information.

In situ monitoring of Pb(II) using Pb(II) IIPs and potentiometric method equipped with cost-free VLC communication system

Grahadi Ganang Aditya
Sriwijaya University
Sahat Maruli Tua Haloho
Sriwijaya University
Idha Royani
Sriwijaya University
Assaidah Assaidah
assaidah@unsri.ac.id

Sriwijaya University

Research Article

Keywords: Pb(II) sensor, IIPs, potentiometry, water monitoring, Arduino, Visible Light Communication

Posted Date: November 12th, 2026

DOI: https://doi.org/10.21203/rs.3.rs-10786862/v1

License: This work is licensed under a Creative Commons Attribution 4.0 International License.
Read Full License

Additional Declarations: No competing interests reported.

RESEARCH ARTICLE

In situ monitoring of Pb(II) using Pb(II) IIPs and potentiometric method equipped with cost-free VLC communication system

Grahadi Ganang Aditya[1], Sahat Maruli Tua Haloho[2], Idha Royani[3], Assaidah[4*]

1Physics Department, Sriwijaya University, South Sumatera, Indonesia; grahadiganangaditya@gmail.com
2Physics Department, Sriwijaya University, South Sumatera, Indonesia; sahathaloho02@gmail.com
3Physics Department, Sriwijaya University, South Sumatera, Indonesia; idharoyani@unsri.ac.id
4Physics Department, Sriwijaya University, South Sumatera, Indonesia; assaidah@unsri.ac.id

*Correspondence email: assaidah@unsri.ac.id

ABSTRACT

Heavy metals such as lead (Pb) pose serious health risks due to their bioaccumulation in the human body, while effective in situ monitoring systems for Pb(II) detection remain limited, especially in Indonesia. This study developed a Pb(II) PI–SPI sensor based on Pb(II) ion-imprinted polymers (IIPs) combined with a simple potentiometric system and bidirectional Visible Light Communication (VLC) technology. The system enables real-time Pb(II) measurement up to 100 m away across aquatic environments, with direct data transmission free from internet or data fees. Application in Teluk Seruo Lake, Indonesia, showed that Pb(II) concentration obtained from steady-state analysis using Boltzmann fitting deviated only 6.42% from the analytical flame AAS result. The steady-state Pb(II) concentration was 38.58 ± 1.45 ppm, while data transmitted via VLC showed an average error of 5.17%. Although the sensor required approximately 12 minutes to reach steady state, it remains faster and more practical than conventional laboratory analysis for field applications. The calibration curve exhibited good linearity ($R^2 = 0.98045$) within 0.1–1 ppm, and comparison with extrapolated non-linear (Boltzmann) fitting confirmed that the linear regression method remains valid for higher concentration measurements. The detected Pb(II) concentration in Teluk Seruo was far exceeded both national and World Health Organization (WHO) limits (0.03 and 0.01 ppm), emphasizing the urgent need for continuous monitoring and remediation of heavy metal contamination in aquatic ecosystems.

Keywords: Pb(II) sensor, IIPs, potentiometry, water monitoring, Arduino, Visible Light Communication

1. Introduction

Heavy metals and metalloids are toxic, persistent, and resistant to natural degradation, making them dangerous environmental pollutants that require precise detection (Y. Qin and Y. Tao, 2022). Their accumulation from sources like industrial waste and pesticides poses serious health risks (C. K. Swain, 2024; Y. Permatasari & M. M. Sianita, 2025; A. E. Noor et al, 2023). Once released as soluble compounds, these metals remain in the environment, causing long-term contamination of soil, water, and sometimes air (M. Rezapour, 2022). Various types of heavy metals have been identified as major contaminants in aquatic environments, including iron (Fe), nickel (Ni), copper (Cu), zinc (Zn), chromium (Cr), cadmium (Cd), mercury (Hg), arsenic (As), manganese (Mn), and lead (Pb) (Y. Qin and Y. Tao, 2022; C. K. Swain, 2024; Y. Permatasari & M. M. Sianita, 2025; A. E. Noor et al, 2023; I. Oladimeji et al, 2020; A. Singh et al, 2022).

Among various heavy metals, lead is one of the most toxic heavy metals (Y. Permatasari & M. M. Sianita, 2025; E. L. Ungureanu & G. Mustateta, 2022; K. Raj and A. P. Das, 2023). Hence, effective in situ monitoring and detection of Pb(II) concentrations is crucial to ensure the protection of human health and aquatic environments (Y. Fang et al, 2024; M. Hasan et al, 2023). Conventional analytical techniques commonly used for the detection of heavy metals, including lead (Pb(II)), comprise X-ray fluorescence spectrometry (XRF), inductively coupled plasma atomic emission spectrometry (ICP-AES), inductively coupled plasma mass spectrometry (ICP-MS), and atomic absorption spectrometry (AAS) (G. Li et al, 2022; M. R. Mehrasebi et al., 2023; Y. Fan et al., 2020; M. Hasan et al, 2023). Absorption has emerged as a simple, efficient, and cost-effective approach for detecting Pb(II), particularly at low concentrations. Its widespread application in wastewater monitoring is supported by the method's sensitivity, reusability of adsorbents, and suitability for on-site analysis (G. Li et al, 2022; S. Cheng et al, 2022; W. Wu et al, 2022; E. Radha et al., 2021). In contrast, conventional spectroscopic methods such as AAS, despite their high sensitivity, selectivity, and accuracy, are often hindered by high costs, bulky instrumentation, and the requirement for skilled operators. These offline, laboratory-based techniques also involve sample transport from treatment sites, which can lead to degradation and delays, thus limiting their applicability for in situ and real-time monitoring (M. Hasan et al., 2023; G. Li et al, 2022; Y. Fan et al., 2020). Therefore, the development of a low-cost, accurate, and rapid analytical method for real-time, in situ monitoring of trace Pb(II) ions is essential for effective contaminant control (Y. Fan et al., 2020; M. Hasan et al, 2023).

Development of Pb(II) sensors have been done including solid-state ion selective membrane (S-ISM), voltametric, composite, colorimetric, electrochemical, and potentiometric sensor. Nevertheless, S-ISM have complexity in fabrication because it needs carbon cloth using active material to modify the electrode (Y. Fan et al., 2020). Voltametric method, susceptible to electrical interference from complex heavy metals at detection environment (G. Li et al, 2022). Composite sensor, have limitation absorbance of Pb(II) ions at maximum pH 7.0 (M. S. Salman et al., 2020). Colorimetric sensor, although the result from Pb(II) detection is visible directly from the change of its color, it can be challenge if the water sample is muddy (L. Xia et al, 2024). Electrochemical sensor, have length and costly preparation that limited the reproducibility and sustainability. Moreover, every electrochemical application, the electrodes need polishing and cleaning frequently which limited sensor performance (J. Jjagwe et al, 2024). Given the numerous limitations of existing Pb(II) sensors, particularly in direct detection within aquatic environments, this study had explored and designed in-situ Pb(II) sensor with simple fabrication, selective to the Pb(II) ion, and only use simple potentiometric instrumentation.

The Pb(II) sensor is developed by Ion Imprinting Polymers (IIPs) material since they are able to recognize ion selectively with high accuracy, can be utilized as filtering media, and as well as for the detection of target ion concentrations (X. Zhou et al, 2022; M. Du et al., 2024; L. Wang et al., 2022; X. Cai et.al., 2014). Using potentiometric instrumentation, the Pb(II) sensor generates a potential difference due to the Pb(II) ion movements which captured by IIPs Pb(II) material containing specific cavities for Pb(II) Ion (M. Rezapour, 2022; I. Royani et al, 2019). Variations of Pb(II) concentration will result in corresponding changes in the potential difference (Y. Fan et al, 2020; M. Çıtlakoğlu & Z. Yolcu, 2023; O. Gholipour et al, 2025). In this study, linear correlation between potential difference (V) and Pb(II) concentration (0.1 – 1 ppm) was established. The potential difference was measured automatically using microcontroller Arduino UNO R3 and connected to the ADS1220 which is 24-bit resolution Analog to Digital Conversion (ADC). ADS1220 used to enhance potential difference measurement precision since Arduino UNO R3 has a resolution of only 10 bits. The Pb(II) sensor is also equipped with a cost-free wireless data communication system based on visible light communication (VLC) technology.

In this work, VLC would be performed in order to Pb(II) can be measured in the middle of aquatic environment (e.g. lake) and the measurement result will be known by user on the shore. As a wireless communication technology, VLC has some advantages compare to radio frequency (RF). First, VLC is free from

electromagnetic interference. Second, it has wide and free-license bandwidth. Third, VLC offers more secure and independent communication because it's hard to interference VLC. Fourth, VLC has power saving advantage than RF (P. Sikder et al, 2025; T. Yu et al, 2021; J. Lian et al, 2019). With all that advantages, there is still not much research has been done to perform VLC as communication system for water surface or underwater monitoring data sensor.

H. Ibraiwish (2024) implemented VLC to collect data from the LED-Based grow light agriculture systems with 5 m link distance using LED as transmitter and photodetector as receiver. Another industrial application, VLC most applicable on health system (D. Iturralde et al, 2024; V. Kavitha et al, 2024); underground mine environment (D. Iturralde et al, 2024; A. RayChowdhury et al, 2021); indoor positioning (Y. Almadani et al, 2020; J. Li et al, 2024); vehicle to vehicle communication (P. Sharda et al, 2022 ; N. M. Okasha & F. A. Newagy, 2024); and all that application using LED as transmitter. In addition to LED, VLC can also utilize laser as transmitters (used in this study) which provide enhanced performance compared to LED, primarily due to their higher optical output and greater beam intensity (S. U. Rehman et al, 2019). To complete VLC system for Pb(II) sensor data, our work used modified solar cell as receiver than another receiver like photodetector, light dependent resistor (LDR) and photodiode because solar cell has wider field of view (FOV) that can provide a large detection area (O. Alkhazragi et al, 2023). Previously, related research has been done by Assaidah (2025) to measure pH and temperature data which combined VLC and RF communication. Although the VLC was limited to perform in maximum 35 m link distance and sunlight intensities <1000 lux (night), yet in this study, using such system, the Pb(II) sensor successfully detected Pb(II) concentrations and transmitted the data over a distance of up to 100 meters; also, it was able to work at the day time after some modification at the receiver side.

In the following, this paper presents: (1) the design and working mechanism of a Pb(II) sensor based on a simple potentiometric instrumentation approach; (2) data processing and calibration results of Pb(II) measurement using Arduino UNO R3; (3) the hardware and software configuration of the VLC system; (4) VLC testing to determine the maximum link distance and data rate using a 2-PWM modulation scheme; and (5) field validation of the integrated Pb(II) sensor system. It is hypothesized that the proposed PI–SPI sensor combined with VLC communication can provide reliable Pb(II) concentration measurements that are comparable to those obtained by the AAS method, while offering advantages in portability, cost-efficiency, real-time and *in-situ* monitoring. This

work thus demonstrates the potential of combining ion-imprinted polymer sensors with optical communication for practical environmental monitoring applications.

2. Materials and methods

2. 1. Fabrication of Pb(II) Ion Imprinted Polymers (IIPS)

Pb(II) Ion Imprinted Polymers (IIPS) in this study was fabricated by (S. M. T. Haloho et al, 2022) with the following procedure. Lead(II) nitrate ($Pb(NO_3)_2$) was used as the template ion for the formation of Pb(II)-imprinted polymers (IIPs). Methacrylic acid (MAA, $C_4H_6O_2$) served as the functional monomer, while ethylene glycol dimethacrylate (EGDMA, $C_{10}H_{14}O_4$) was used as the crosslinking agent. Methanol (CH_3OH) acted as a protogenic solvent, and benzoyl peroxide (BPO, $C_{14}H_{10}O_4$) was employed as the polymerization initiator. Distilled water and deionized water were used as solvents and cleaning agents throughout the experiment. Hydrochloric acid (HCl) was utilized for the extraction of Pb(II) ions from the polymer matrix, and acetic acid (CH_3COOH) was applied as a gelatin solvent. Poly-vinyl-alcohol (PVA) and gelatin ($C_{102}H_{151}N_{31}O_{39}$) were used as precursors and reagents in the electrospinning process. All chemicals were of analytical grade and used without further purification.

2. 1. 1. Synthesis of Pb(II) Polymer

All glassware and materials were prepared prior to synthesis. A mixture consisting of 0.3 g of $Pb(NO_3)_2$, 35.2 mL of methanol, 0.6 mL of methacrylic acid (MAA), 9 mL of ethylene-glycol-dimethacrylate (EGDMA), and 0.1 g of benzoyl peroxide (BPO) was prepared in a beaker glass. The solution was homogenized using a magnetic stirrer for 30 minutes at 65°C on a hot plate to ensure complete mixing of the components. After homogenization, the mixture was cooled at −5°C for 1 hour in a freezer to initiate pre-polymer complex formation. The resulting mixture was then subjected to a polymerization process in a furnace through a stepwise heating program: 75°C for 3 hours, 80°C for 2 hours, and finally 85°C for 1 hour. The obtained solid polymer was designated as Pb(II) polymer.

2. 1. 2. Preparation of Pb(II) Ion Imprinted Polymers (Pb(II) IIPs)

The synthesized Pb(II) polymer was ground using a mortar and pestle until a fine powder obtained. The powdered polymer was washed sequentially with methanol and deionized water, each repeated five times, to remove

unreacted residues. Subsequently, Pb(II) ions were extracted from the polymer matrix using 1M HCl solution with a volume ratio of 20×50 mL for 4 hours under stirring. The extraction process was continued until no Pb(II) was detected, confirming the formation of Pb(II)-ion imprinted polymer (Pb(II)-IIPs). The obtained Pb(II)-IIPs was washed with deionized water until the filtrate reached a neutral pH, then dried in an oven at 60°C for 3 hours.

2. 2. Fabrication of Pb(II) sensor based on Pb(II) IIPs using simple potentiometric instrumentation (PI-SPI)

Pb(II) PI-SPI sensor consist of two solutions which is 50 mL Pb(II) IIPs internal solution and 50 mL test solution. The internal solution was prepared by mixing 0.2 g of Pb(II) IIPs material with 17 mL of 0.03 M HCl, 17 mL of 0.02 M KCl, and 17 mL of a 12.5 ppm Pb(II) solution. A 17 mL solution of 0.03 M HCl was prepared by diluting 0.04 mL of 12.4 M concentrated HCl (Sigma-Aldrich) with 16.96 mL of distilled water. A 0.02 M KCl solution (17 mL) was prepared by dissolving 0.02533 g of KCl (Merck) in 17 mL of distilled water. A 17 mL solution of 12.5 ppm Pb(II) was prepared by diluting 0.425 mL of a 500 ppm Pb(II) stock solution with 16.575 mL of distilled water. Prior to this, a 500 ppm Pb(II) stock solution was prepared by dissolving 0.08 g of $Pb(NO_3)_2$ (Sigma-Aldrich) in 100 mL of distilled water.

The test solution is the sample in which the concentration of Pb(II) ions will be detected, such as river or lake water. For the calibration process, test solutions were laboratory prepared with concentrations ranging from 0.1 – 1 ppm, each with a volume of 10 mL, by diluting a 500 ppm Pb(II) stock solution with distilled water.

Fig. 1 shows the Pb(II) PI-SPI sensor fabricated in this study. Potentiometric instrumentation is carried out using an Al electrode as working electrode (WE) and an Ag/AgCl electrode as reference electrode (RE). The WE is placed in the internal solution, while the RE is placed in the test solution. These two solutions are connected by a salt bridge, which in this study is implemented using filter paper. This setup allows the migration of ions from the test solution to the internal solution. The Pb(II) ions that migrate into the internal solution are selectively captured by the Pb(II) ion-imprinted polymers (IIPs), and this ion movement generates a potential difference across the system. The potential difference arises due to both the concentration gradient between the two solutions and the selective binding of Pb(II) ions by the IIPs. As a result of this ion migration, the internal solution gains a net positive charge, while the test solution loses charge. Consequently, the aluminum electrode functions as the negative pole, and the Ag/AgCl electrode serves as the positive pole during the potential difference measurement using the Arduino UNO R3.

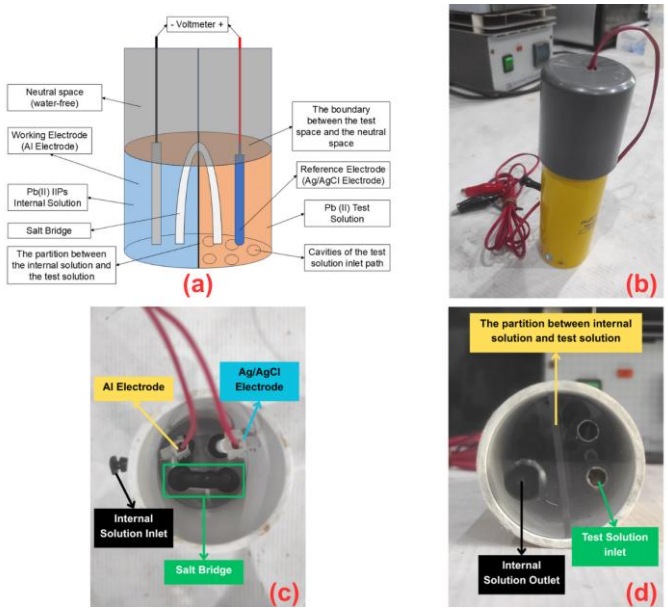


Fig. 1. Pb(II) PI-SPI sensor. (a) Design; (b) Perspective view; (c) Top view; (d) Bottom view

2.3. Calibration test of Pb(II) PI-SPI sensor

Pb(II) PI-SPI sensor calibrated using various concentration of Pb(II) test solution: 0.1, 0.2, 0.3, 0.4, 0.5, 0.6, 0.7, 0.8, 0.9, and 1 ppm. The test solution, each with a volume of 10 mL, was laboratory prepared by diluting a 500 ppm Pb(II) stock solution with distilled water. Potential difference detected by connected Ag/AgCl electrode as positive pole and Al electrode as negative pole to the ADS1220 that connect to Arduino UNO R3 using SPI communication. As a 24-bit resolution ADC, ADS1220 can detect a very low potential difference and it is important to process data precisely and accurately. The ideally potential difference resolution in this set up by using 2.048 V voltage reference is 0.122 µV.

2.4. Hardware and software design of VLC system

VLC system equipped with this Pb(II) PI-SPI sensor will do bidirectional communication using two modems, named Modem I and Modem II (Fig.2). Modem I will be placed at the side while Modem II will be placed in the middle of aquatic environment. Generally, Modem I and Modem II have similar component which is Arduino UNO R3 as microcontroller, 35 mW red laser diode as transmitter, IRF520N module as laser controller, and solar cell 5 V/220 mA as receiver. In additional, Modem I has push button as controller to take data from Modem II and microSD to save data from Modem II while Modem II has ADS1220 as high resolution potential differencial

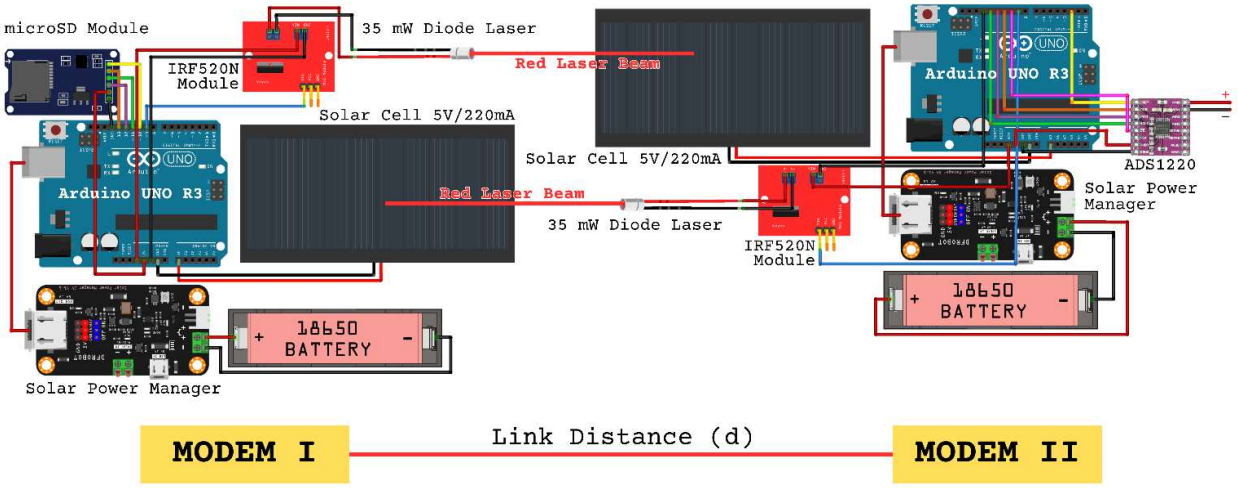


Fig. 2. Hardware design of Pb(II) PI-SPI sensor VLC system.

detector from Pb(II) PI-SPI. All components linked to Arduino UNO R3 each modem. 35 mW red laser diode linked to IRF520N module, while IRF520N module linked to digital pin (D9). IRF520N module will control 35 mW red laser diode by using pulse width modulation (PWM) to send modulated data. The data send in binary follow American Standard Code for Information Interchange (ASCII) will be detected by solar cell 5 V/ 220 mA which is connected to analog pin (A0). Push button linked to digital pin (D4) and microSD module will linked to SPI pin on Arduino UNO R3 Modem I, while ADS1220 linked to SPI pin on Arduino UNO R3 Modem II.

Software design of VLC system embedded modulation and demodulation program to Arduino UNO R3 board using Arduino IDE 2.3.4 application. 2-PWM 50 ms modulation had been chosen in this system with a 20 Hz laser frequency (Eq. 1) and produce 40 bps data rate (Eq. 2). Respectively, although the data rate is low, it is enough for Pb(II) PI-SPI sensor data transmission.

$$Laser\ Frequency\ (Hz) = \frac{1\ (s)}{pulse\ width\ (s)} \quad (1)$$

$$Data\ rate\ (bps) = Number\ of\ bits \times Laser\ Frequency \quad (2)$$

The 2-PWM modulation means the binary code will send two bits every pulse width. Modulation program consisted of 3 step programming: (1) initialize used pulse width, (2) modulate character data to binary code follow ASCII code, (3) send 2 bits data every pulse width. As same as modulation program, the demodulation program also consist of 3 step programming: (1) initialize pulse width from the 2 bits packet data, (2) demodulate received pulse width to packet bits, (3) demodulate received pulse width to character.

2.3. Experimental set up

Once the hardware and software designs were completed, the experiment was carried out in the laboratory to make sure the system work properly, and after that field experiment will be held. Modem I will send signal through laser to Modem II after Modem I push button was pressed by user. The signal received by Modem II will command Modem II to send back Pb(II) PI-SPI sensor data to Modem I. Data collected by Modem I will be stored in the microSD. In order to Pb(II) data can collected by Modem II in the middle of the water, a buoy was made previously. In this study, field experiment was placed at Teluk Seruo Lake, Ogan Ilir Regency, South Sumatera, Indonesia. Teluk Seruo Lake acts as a water retention basin in the dry season and has been utilized as a tourism site since 2015. Based on Government Regulation of the Republic of Indonesia Number 22 of 2021 on the Implementation of Environmental Protection and Management, as water retention basin and tourism site, the threshold limit for dissolved lead (Pb) is set at 0.03 mg/L. To the best of the author's knowledge, no reports have been found regarding the concentration levels of Pb(II) in Teluk Seruo Lake, either based on sample testing or automatic monitoring data.

Figure 3 shows the internal hardware configuration of Modem I and Modem II. The solar cell, which functions as the receiver, has been modified by adding a protective cover with dimensions of 11 × 5 × 20 cm. This cover functions as a sunlight shield to minimize optical noise that can interfere the laser beam detection. Under sunlight intensities exceeding 1000 lux, the solar cell is unable to reliably differentiate between the modulated laser signal and ambient sunlight, potentially causing communication failure. Black was chosen as the cover color due to its ability to absorb light, thereby minimizing reflection and preventing interference with the laser signal. The

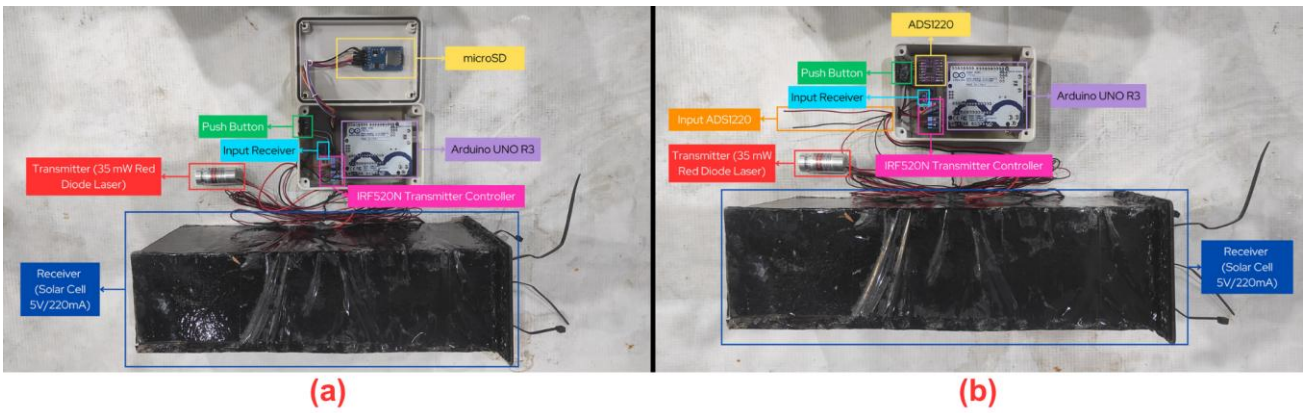


Fig. 3. Hardware circuit. (a) Modem I; (b) Modem II.

modification significantly enhances the solar cell's ability to detect laser signals during daytime conditions, thereby overcoming the limitation of Visible Light Communication (VLC) systems that typically restrict operation to night time environments (Assaidah et al, 2025). An additional advantage is that the modification requires only a simple structural change, without the need for complex and expensive optical filtering.

3. Results and Discussion

3.1. Pb(II) IIPs Characterization

The surface morphology of the Pb(II) polymer and Pb(II) ion-imprinted polymer (IIPs-Pb(II)) was analyzed using a Scanning Electron Microscope (SEM) at a magnification of 250 times. The SEM images revealed distinct differences between the two materials. The non-imprinted Pb(II) polymer (Fig. 4(a)) exhibited a relatively dense and compact morphology with fewer visible pores, while the IIPs-Pb(II) material (Fig. 4(b)) displayed a more porous and heterogeneous surface structure. This increased porosity in IIPs-Pb(II) was attributed to the template extraction process, which successfully created imprinted cavities corresponding to the Pb(II) ions. Furthermore, the pore diameter distribution of both materials, presented in Fig. 4(c), indicates that the majority of the cavities were formed at the nanometer scale, within the range of 1–100 nm. Such nanoscale cavities confirm that the polymerization and imprinting processes were effectively achieved, providing specific recognition sites for Pb(II) ions. These morphological features are consistent with successful ion imprinting, which enhances both the adsorption capacity and selectivity of the Pb(II) IIPs sensor.

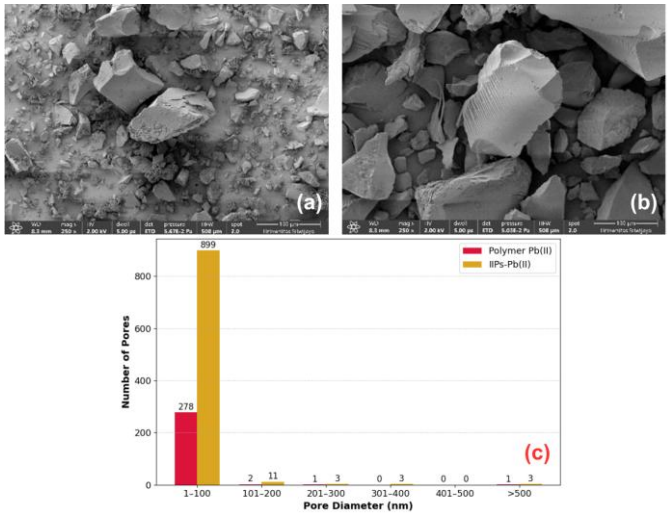


Fig. 4. (a) SEM analysis of Pb(II) polymer; (b) SEM analysis of Pb(II) IIPs; (c) Pore size distribution of Pb(II) polymer and Pb(II) IIPs. *The image and data were courtesy from (Sahat et al, 2024)*

3.2. Pb(II) PI-SPI Sensor Calibration

The Calibration of the Pb(II) PI-SPI sensor was carried out using various Pb(II) solutions with concentrations ranging from 0.1 to 1 ppm, with an interval of 0.1 ppm. The sensor detects the potential difference (V) through potentiometric instrumentation. The ADS1220, a high-resolution 24-bit ADC, was used to measure this potential difference, with the A0 pin connected to the Ag/AgCl electrode and the A1 pin to the Al electrode. Prior to its application in the sensor system, the ADS1220 was calibrated using a power supply to measure voltages ranging from 0.1 to 1 V. A FLUKE 17B+ digital multimeter was employed as a reference instrument during this calibration process to ensure measurement accuracy. Figure 5(a) show the calibration result of ADS1220. The calibration of the ADS1220 resulted in an R^2 value of 0.99997, indicating an excellent correlation between the reference input and the measured output, thus confirming its readiness for use.

The Pb(II) PI-SPI sensor calibration was then performed by measuring each concentration 10 times, yielding an R^2 value of 0.98045 as shown in Fig. 5(b). This value indicates a very strong correlation between the sensor response and the analyte concentration, albeit slightly below the ideal threshold of 0.99. This minor deviation may be attributed to small variations in repeated measurements or slight inaccuracies in the preparation of standard solutions. Nevertheless, the result reflects a reliable calibration performance and is deemed sufficient for quantitative analytical applications. Figure 5(b) also shows the linearity equation from Pb(II) concentration and voltage (v) measured with ADS1220, the ADC (analog-to-digital-converter) component with 24 bits of resolution, to detect a very small potential difference from the Pb(II) concentration for increasing the sensor accuracy. The

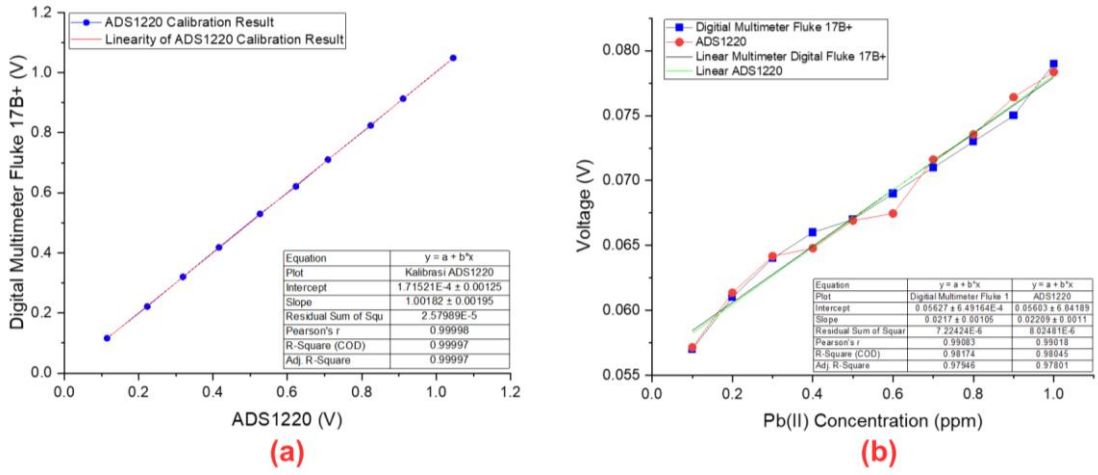


Fig. 5. (a) Calibration result and correlation between ADS1220 and digital multimeter; (b) Correlation between Pb(II) concentration (ppm) and voltage (V).

linearity equation is $y=0.05603+0.02209x$ where $\boldsymbol{y}$ as voltage (v) and $\boldsymbol{x}$ as Pb(II) concentration. Hence, using the equation, we can calculate Pb(II) concentration from the voltage (V) values using Eq. 3.

$$Pb(II)\ concentration\ (ppm) = \frac{Voltage\ (V) - 0.05603}{0.02209} \quad (3)$$

3.3 VLC link distance and data rate between Modem I and Modem II

Successful data transmission depends on the bit error ratio (BER) value. BER should below 3.8 x 10^{-3} for successful data transmission, meaning that out of 10k transmitted bits, a maximum of 38 bits error is tolerable. However, at the low data rate transmission (<100 bps), BER must be 0 to perform successful data transmission and BER will be 1 (failed transmission) when there is bit error even only 1 bit. Figure 6(a) show successful data transmission over 1 meter link distance at various laser frequency using 1-PWM and 2-PWM modulation. The 2-PWM modulation at 20 Hz was selected as it demonstrated the most effective performance for VLC data transmission, as shown in Fig. 6(a). Using this modulation scheme, the communication link was successfully established over a distance of up to 100 meters (Fig. 6(b)).

Bidirectional communication between Modem I and Modem II was achieved and compared to the previous study where this work extended the maximum link distance as shown by Table 1. Although the data rate is decrease, but the link distance up to 100 m. For real-time applications, the data transmission is sufficient since only six characters (48 bits) are sent, resulting in a waiting time of just 1.2 seconds. Besides that, 2-PWM modulation is a simpler programming code compared to another modulation scheme.

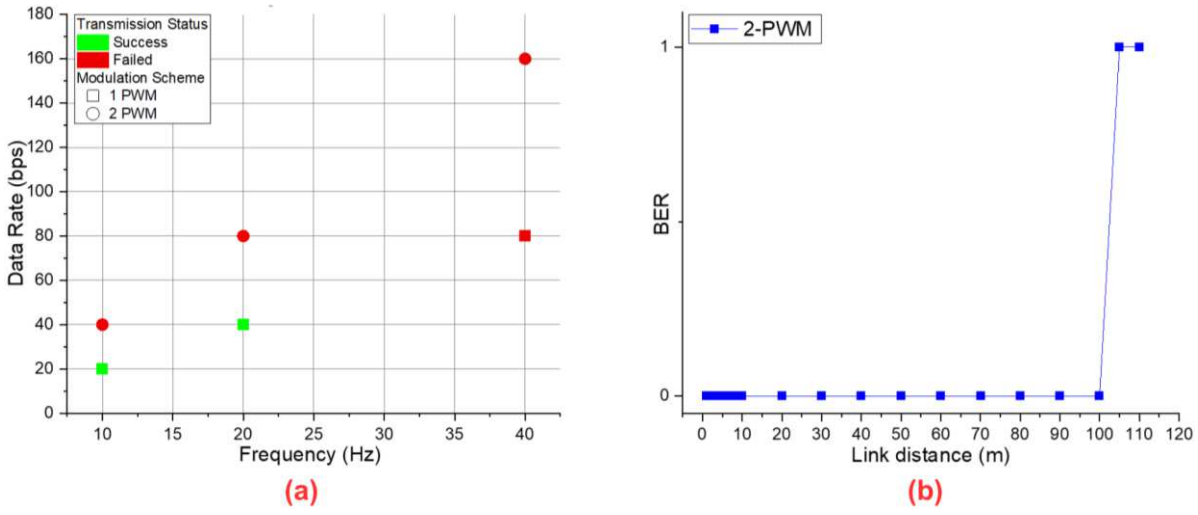


Fig. 6. (a) BER performance at various link distance using 2-PWM; (b) BER performance at various link distance using 2-PWM.

Table 1. Comparison of VLC performance between previous study and this study

Transmitter (Laser)	Receiver	Modulation	Data rate	Link distance	Transmission Medium	Author
Diode laser	Photodiode	16-QAM-OFDM	12.5 Gbps	5 m	Air	C. H. Chang et al. 2014
		16-QAM-OFDM MIMO Paralel 8 Tx and Rx	100 Gbps			
Diode laser	Photodiode	64-QAM-DMT	25 Gbps	10 m	Air	WC Hang et al. 2018
RGBV diode laser	Photodiode	OFDM	35 Gbps	4 m	Air	H. Chun et al. 2019
Red diode laser	Photodiode	OOK-NRZ	4.5 Gbps	30 cm	Air	MHM Shamim et al. 2019
Blue diode laser			3.5 Gbps			
Red and blue diode laser			8 Gbps			
RGBV diode laser	Photodiode	OFDM	26,228 Gbps	2 m	Air	CW Chow et al. 2020
GaN laser	Photodiode	-	2.5 Gbps	10 m	Air and optical fibre	SP Najda et al. 2022
Red diode laser	Polycristalline solar cell 6V/500mA	1-PWM	20 bps	35 m	Air	Assaidah et al. 2025
		2-PWM	40 bps	15 m		
Red diode laser	Polycristalline solar cell 5V/220mA	2-PWM	40 bps	100 m	Air	This Study

3.4. In-situ Pb(II) monitoring at Teluk Seruo Lake

In-situ monitoring was conducted on May 10, 2025. The Pb(II) PI-SPI sensor at Modem II measured the potential difference (V) every 0.5 seconds from the moment the sensor was placed in the water until a steady-state potential was reached. The measurement lasted for 7126 seconds (approximately 118 minutes) to analyze the signal behavior. As shown in Fig. 7, the data exhibited fluctuating values as a response to the migration of Pb(II) ions from the test solution (Teluk Seruo Lake water) into the internal solution, where the ions were captured by Pb(II) IIPs, resulting a potential difference. The measured potential difference was converted into Pb(II) concentration using Eq. (3). The concentration of Pb(II) increased over time and eventually reached a steady state. Sigmoidal analysis using the Boltzmann function was performed to determine the rise time, the onset of the steady-state condition, and the corresponding Pb(II) concentration at steady state. The rise time was observed to begin at 3 seconds and reached steady state at 714.48 seconds, resulting in a total duration of 717.48 seconds (approximately 12 minutes). From 714.48 seconds onwards, the data stabilized, indicating the onset of steady-state conditions as confirmed by the Boltzmann analysis. At steady state, the Pb(II) concentration was 38.58 ppm, with a standard deviation 1.44732 ppm. The steady state requires over 714 seconds because Pb(II) ions need time to move from the test solution (lake water) to the internal solution through the salt bridge. This relatively long response time is mainly caused by the slow diffusion of Pb(II) ions across the salt bridge, which limits mass transfer between the two solutions. The high Pb(II) concentration also contributes to this delay, as it takes longer for the system to reach saturation.

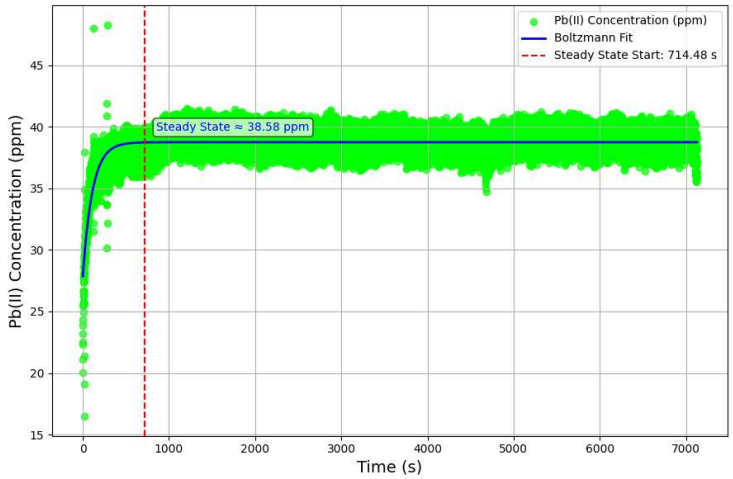


Fig. 7. Variation of Pb(II) concentration (ppm) over time during in-situ monitoring.

The potentiometric response observed during the in-situ measurement can be explained by the selective interaction between Pb(II) ions and the functional groups of the IIPs. During the polymerization process, specific binding sites are formed that are structurally and chemically complementary to Pb(II) ions. When the sensor is immersed in lake water, Pb(II) ions diffuse into these imprinted cavities and form coordination bonds with the carboxyl groups of methacrylic acid (MAA), leading to a measurable change in potential. As Pb(II) binding sites become progressively occupied, the potential gradually increases until equilibrium is achieved, corresponding to the steady-state condition observed at approximately 714 seconds. This mechanism confirms that the potential stabilization reflects the completion of Pb(II) ion adsorption by the IIPs layer. The good reproducibility and clear steady-state behavior indicate that the IIPs film provides selective recognition toward Pb(II) ions, ensuring reliable potentiometric response under real environmental conditions. Therefore, the observed potential evolution and steady-state response demonstrate the effectiveness of the Pb(II) IIPs layer in facilitating selective and stable Pb(II) ion detection during in-situ operation.

The Pb(II) concentration data were transmitted from Modem II to Modem I after Modem I initiated a request signal to Modem II. Figure 8 shows the position of the PI-SPI sensor connected to Modem II, which was deployed in the center of Teluk Seruo Lake. The communication system between Modem I and Modem II in this study followed the method previously described in (Assaidah et al, 2025), with several modifications. One notable



Fig. 8. PI-SPI sensor placement inside the lake connected to Modem II

adjustment involved the use of a modified solar cell as the photodetector and another modification was the communication distance, which was set to 30 meters—matching the span from the center to the shore of Teluk Seruo Lake. Transmission data had been succeeded as well as laboratory test result up to 100 m link distance.

The data received by Modem I were stored on a microSD card for user access. As a transmitter, the 35mW red laser diode provides highly focused light and stable optical power, outperforming LEDs whose emission is more divergent. The modified solar cell with a black cover effectively mitigated daytime transmission failures caused by sunlight noise exceeding 1000 lux, without requiring complex optical filtering. In this study, Pb(II) measurement and data transmission were conducted between 9:30 a.m. and 11:30 a.m. The VLC communication system demonstrated robust performance under varying weather conditions, including rain and strong sunlight, as long as the red laser diode and solar cell remained directly aligned. Data transmission was still achievable even at noon (~12 p.m.), when ambient light intensity was highest. To minimize interference from water surface fluctuations, the laser was mounted on a fixed pole, ensuring stable optical alignment and reliable transmission. These findings confirm that the VLC setup is sufficiently resilient for outdoor environmental monitoring applications. The in-situ Pb(II) measurements data obtained via the PI–SPI sensor was compared with laboratory-based Flame AAS results to assess accuracy and reliability. Table 2 presents Pb(II) concentrations from Flame AAS, steady-state measurements, and VLC data.

Table 2. Pb(II) concentration of Teluk Seruo Lake using flame AAS, steady state data, and VLC.

Flame AAS (ppm)	**Steady state data (ppm)**	**Error (%)**	**VLC (ppm)**	**Error (%)**
			39.12	7.91
			37.8	4.27
			38.86	7.20
36.25	38.58	6.42	38.89	7.28
			37.58	2.84
			37.73	4.08
			37.21	2.64
		Average		5.17

The Pb(II) concentration measured using the flame AAS method was used as a reference value to calculate the measurement error from the steady-state data analysis and the Pb(II) concentration transmitted using VLC. The Pb(II) concentration obtained from the steady-state data showed a 6.42% error compared to the flame AAS result. Although the value exceeded the acceptable error threshold (5%), it still represents a relatively low deviation of 1.42%. This measurement result also validates that, although the calibration was performed at low concentrations (0.1–1 ppm), the sensor demonstrates good performance in measuring higher concentrations due to its linearity. Figure 9 shows the comparison between extrapolated calibration analysis using linear and non-linear regression, confirming that the method used in this study, linear regression, is valid.

Pb(II) concentration received by user on the side (Modem I) that is sent from the middle of the lake (Modem II) was sent every 15 minutes after user push the start button at Modem I. As can be seen at Table 2, the Pb(II) concentration received by user had average error of 5.17% from seven times data collection with highest error 7.91% and lowest error 2.64%. The transmitted data also varied by approximately 1.44 ppm from the steady-state concentration (38.58 ppm), based on the standard deviation. The observed errors can be attributed mainly to instrumental and electronic noise besides reference electrode drift. Small fluctuations in the analog-to-digital converter (ADC) and amplifier circuitry may have introduced minor variations in the recorded potential, particularly during the steady-state determination. Additionally, slight drift in the Ag/AgCl reference electrode potential due to changes in chloride concentration or junction stability could shift the baseline potential over time, resulting in small systematic deviations. Despite these factors, the overall error remains within an acceptable range, indicating a stable and reliable sensor performance.

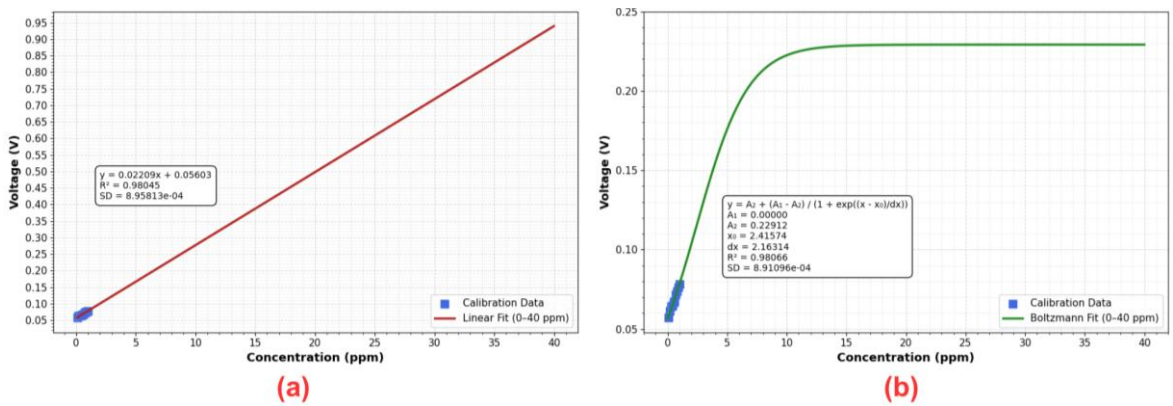


Fig. 9. (a) Linear calibration curve; (b) Non-linear calibration curve (Boltzman Fit).

Furthermore, the Pb(II) measurement using the PI–SPI sensor exhibited a significantly faster response, requiring only about 12 minutes to reach steady state compared with the flame AAS method, which typically requires about one week for analysis. The system can also be directly deployed in the field. The total prototype cost is less than USD 185 where the integration with the VLC system, data transmission from the lake center to the shore can be achieved without internet connectivity or data packages. In contrast to previous studies, which generally focused on Pb(II) detection in controlled laboratory environments or limited to pre-collected water samples, this study successfully demonstrates a fully *in-situ* application of a Pb(II) sensor integrated with a VLC-based wireless data transmission system. This integration represents a significant advancement because it enables real-time and in-situ Pb(II) monitoring in aquatic environments without relying on conventional wireless communication technologies, which are often unreliable or unavailable in remote field locations. The novelty of this work lies in the combination of IIPs based potentiometric sensing and VLC within a single low-cost and field-deployable platform. This configuration not only improves analytical practicality by reducing analysis time and operational cost but also introduces a new paradigm for environmental monitoring where chemical sensing and data transmission are optically integrated. Therefore, this work provides a new approach to real-time heavy metal monitoring systems, particularly for Pb(II) in natural water bodies. Table 3 presents a comparison between this study and previous works on Pb(II) sensors.

Table 3. Comparison between this study and previous works on Pb(II) sensors.

Sensor types	**LOD (µg/L)**	**10-LOQ (µg/L)**	**Response time**	**Selectivity**	**Cost**	**Field applicability**	**Source**
Pb(II) Ion Imprinted Polymers – Potentiometric sensor	93	3100	714 s	Selective using Pb(II) IIPs material	< $185 for full system with VLC	In Situ - Teluk Seruo Lake	This study
Solid-state ion selective membrane	-	-	10 s	Selective	< $1 each sensor	Wastewater	Y. Fan et al. 2020
Voltammetric sensor	0.074	-	300 s	Selective	-	Tongxin lake water sample, Tap water sample, Milk sample	G.Li et al. 2022
Composite sensor	0.24	-	-	Selective to Pb(II) ions with the test of metal ions such as Zn(II), Ba (II), Al(III), Fe(III), Mg(II), Ca(II), Ni(II),	-	30 mL water sample	M. S. Salman et al. 2021

				Ag(I), K(I), Na(I), Mn(II), Hg (II), Bi(III)			
Colorimetric sensor	2.2	7.34	100 s	Selective, Other metal ions such as Al(III), Cr(VI), Cu(II), Ag(I), Hg(II), Cd(II), and As did not cause any significant change in color or absorbance (<0.1).	-	Water sample	L. Xia et al. 2024
Electrochemical sensor	0.02	-	100-400 s	Selective	-	Water sample	J. Jjagwe et al. 2024

This Pb(II) concentration measurement at Teluk Seruo Lake using the PI–SPI sensor also provided insight into the alarming level of Pb(II) contamination in the lake. According to the Government Regulation of the Republic of Indonesia Number 22 of 2021 on the Implementation of Environmental Protection and Management, the permissible limit for dissolved lead (Pb) in water retention basins and tourism sites is 0.03 mg/L (0.03 ppm). Based on the flame AAS analysis, the Pb(II) concentration in Teluk Seruo Lake reached 36.22 ppm, which is more than 1200 times higher than the national standard. For comparison, the World Health Organization (WHO) (2022) provisional guideline value for Pb in drinking water is 0.01 mg/L (0.01 ppm). Such an extremely high Pb(II) concentration reflects a serious contamination level that could pose significant risks to both the environment and human health. Prolonged exposure to lead-contaminated water is known to impair several vital organs, including the kidneys, liver, nervous, and reproductive systems. It can also interfere with hemoglobin formation and oxygen transport in the blood, leading to anemia and fatigue. Moreover, the accumulation of heavy metals in the human body can weaken the immune system, increase the risk of cardiovascular disorders, and, in severe cases, contribute to the development of various cancers. Therefore, the Pb(II) contamination observed in Teluk Seruo Lake highlights the urgent need for regular environmental monitoring and preventive measures to safeguard public health and the surrounding ecosystem.

4. Conclusion

The developed Pb(II) PI–SPI sensor integrated with a visible light communication (VLC) system offers a reliable, low-cost, and portable solution for in situ monitoring of lead contamination in aquatic environments. Applied to Teluk Seruo Lake, the system measured Pb(II) concentration with only 6.42% deviation from flame AAS results, while data transmission through the dual-PWM VLC link achieved a 30 m range with 5.17% average error,

enabling real-time communication without internet connectivity. The modified solar-cell receiver effectively reduced daylight interference, ensuring stable outdoor operation. Although the sensor required about 12 minutes to reach steady-state, this response time remains significantly faster and more practical than conventional laboratory analyses. SEM characterization confirmed successful Pb(II) imprinting with a porous, homogeneous surface favorable for ion binding. The detected Pb(II) concentration (36.22 ppm) far exceeded both national and WHO limits, highlighting the urgent need for continuous monitoring and remediation. Future work will address selectivity toward competing ions and long-term sensor stability to enhance performance reliability.

Declaration Statement

All authors have read, understood, and have complied as applicable with the statement on "Ethical responsibilities of Authors".

FUNDING

Not Applicable.

References

A. E. Noor et al. (2024). Health risks assessment and source admeasurement of potentially dangerous heavy metals (Cu, Fe, and Ni) in rapidly growing urban settlement. *Environ. Res., vol. 242, no. February*, https://doi.org/10.1016/j.envres.2023.117736

A. RayChowdhury, A. Pramanik, and G. C. Roy. (2021). New approach for localization and smart data transmission inside underground mine environment. *SN Appl. Sci., vol. 3, no. 6*, https://doi.org/10.1007/s42452-021-04589-2

A. Singh et al. (2022). Heavy Metal Contamination of Water and Their Toxic Effect on Living Organisms. *Toxic. Environ. Pollut.*, https://doi.org/10.5772/intechopen.105075

Assaidah et al. (2025). A low-cost bidirectional laser communication system for pH and temperature monitoring of Teluk Seruo Lake, Indonesia. *Meas. J. Int. Meas. Confed., vol. 253, no. April*, https://doi.org/10.1016/j.measurement.2025.117679

C. H. Chang et al. (2014). A 100-Gb/s multiple-input multiple-output visible laser light communication system. *J. Light. Technol., vol. 32, no. 24, pp. 4723–4729*, https://doi.org/10.1109/JLT.2014.2365451

C. K. Swain. (2024). Environmental pollution indices: a review on concentration of heavy metals in air, water, and soil near industrialization and urbanisation. *Discov. Environ., vol. 2, no. 1*, https://doi.org/10.1007/s44274-024-00030-8.

C. W. Chow, Y. H. Chang, L. Y. Wei, C. H. Yeh, and Y. Liu. (2020). 26.228-Gbit/s RGBV Visible Light Communication (VLC) with 2-m Free Space Transmission. *25th Opto-Electronics Commun. Conf. OECC 2020, no. Vlc, pp. 20–22* https://doi.org/10.1109/OECC48412.2020.9273596

D. Iturralde et al. (2024). A New Internet of Things Hybrid VLC/RF System for m-Health in an Underground Mining Industry. *Sensors, vol. 24, no. 1, pp. 1–15*, https://doi.org/10.3390/s24010031

E. L. Ungureanu and G. Mustateta. (2022). Toxicity of Heavy Metals. *Environ. Impact Remediat. Heavy Met.*, https://doi.org/10.5772/intechopen.102441

E. Radha, T. Gomathi, P. N. Sudha, S. Latha, A. A. Ghfar, and N. Hossain. (2021). Adsorption studies on removal of Pb(II) and Cd(II) ions using chitosan derived copoymeric blend. *Biomass Convers. Biorefinery, no. October*, https://doi.org/10.1007/s13399-021-01918-8

G. Li et al. (2022). Low-cost voltammetric sensors for robust determination of toxic Cd(II) and Pb(II) in environment and food based on shuttle-like α-Fe2O3 nanoparticles decorated β-Bi2O3 microspheres. *Microchem. J., vol. 179, no. January, p. 107515*, https://doi.org/10.1016/j.microc.2022.107515

H. Chun, A. Gomez, C. Quintana, W. Zhang, G. Faulkner, and D. O'Brien. (2019). A Wide-Area Coverage 35 Gb/s Visible Light Communications Link for Indoor Wireless Applications. *Sci. Rep., vol. 9, no. 1, pp. 4–11,* https://doi.org/10.1038/s41598-019-41397-6

H. Ibraiwish, M. W. Eltokhey, and M. S. Alouini. (2024). UAV-Assisted VLC Using LED-Based Grow Lights in Precision Agriculture Systems. *IEEE Internet Things Mag., vol. 7, no. 3, pp. 100–105*, https://doi.org/10.1109/IOTM.001.2300122

I. Royani, Assaidah, Widayani, M. Abdullah, and Khairurrijal. (2019). The effect of atrazine concentration on galvanic cell potential based on molecularly imprinted polymers (MIPS) and aluminium as contact electrode. *J. Phys. Conf. Ser., vol. 1282, no. 1,* https://doi.org/10.1088/1742-6596/1282/1/012029

I. Oladimeji et al. (2020). Design and Construction of an Arduino - Based Solar Power Parameter-Measuring System With Data Logger. *Arid Zo. J. Eng. Technol. Environ. Azojete, vol. 16, no. 2, pp. 255–268*.

J. Jjagwe, P. W. Olupot, R. Kulabako, and S. Carrara. (2024). Electrochemical sensors modified with iron oxide nanoparticles/nanocomposites for voltammetric detection of Pb (II) in water: A review. *Heliyon, vol. 10, no. 8,* https://doi.org/10.1016/j.heliyon.2024.e29743

J. Lian, Z. Vatansever, M. Noshad, and M. Brandt-Pearce. (2019). Indoor visible light communications, networking, and applications. *JPhys Photonics, vol. 1, no. 1*, https://doi.org/10.1088/2515-7647/aaf74a

J. Li et al. (2024). VLocSense: Integrated VLC System for Indoor Passive Localization and Human Sensing. *ACM MobiCom 2024 - Proc. 30th Int. Conf. Mob. Comput. Netw., pp. 2022–2027,* https://doi.org/10.1145/3636534.3694729

K. Raj and A. P. Das. (2023). Lead pollution: Impact on environment and human health and approach for a sustainable solution. *Environ. Chem. Ecotoxicol., vol. 5, no. February, pp. 79–85*, https://doi.org/10.1016/j.enceco.2023.02.001

L. Xia, F. Luo, X. Niu, Y. Tang, and Y. Wu. (2024). Facile colorimetric sensor using oxidase-like activity of octahedral Ag2O particles for highly selective detection of Pb(II) in water. *Sci. Total Environ., vol. 915, no. January,* https://doi.org/10.1016/j.scitotenv.2024.170025

L. Wang et al. (2022). A rotary multi-positioned cloth/paper hybrid microfluidic device for simultaneous fluorescence sensing of mercury and lead ions by using ion imprinted technologies. *Journal of Hazardous Materials*, 428, 128165. https://doi.org/10.1016/j.jhazmat.2021.128165

M. Çıtlakoğlu and Z. Yolcu. (2023). Dinuclear Pb(II) monomer complex: Synthesis, characterization, and application of Pb(II) ion-imprinted polymer as a selective potentiometric microsensor. *Polyhedron, vol. 243,* https://doi.org/10.1016/j.poly.2023.116539

M. Du et al. (2024). Application Prospect of Ion-Imprinted Polymers in Harmless Treatment of Heavy Metal Wastewater. *Molecules, 29(13), 3160*. https://doi.org/10.3390/molecules29133160

M. H. M. Shamim et al. (2019). Analysis of optical injection on red and blue laser diodes for high bit-rate visible light communication. *Opt. Commun., vol. 449, no. February, pp. 79–85*, https://doi.org/10.1016/j.optcom.2019.05.034

M. Hasan et al. (2023). Colloids and Surfaces A: Physicochemical and Engineering Aspects Facial conjugate adsorbent for sustainable Pb (II) ion monitoring and removal from contaminated water. *Colloids Surfaces A Physicochem. Eng. Asp., vol. 673, no. June, p. 131794.* https://doi.org/10.1016/j.colsurfa.2023.131794.

M. Hasan et al. (2023). Facial Conjugate Adsorbent for Sustainable Pb(II) Ion Monitoring and Removal from Contaminated Water. *Colloids Surfaces A Physicochem. Eng. Asp., vol. 673, no. June, p. 131794*, https://doi.org/10.1016/j.colsurfa.2023.131794

M. Rezapour. (2022). Pb(II)-Imprinted Polymers for Construction of Lead-Selective Electrochemical Sensors. *Anal. Bioanal. Electrochem., vol. 14, no. 2, pp. 144–159*. Available online: https://www.abechem.com/article_249813.html

M. R. Mehrasebi et al. (2023). Comparison of three digestion methods for determination of lead and cadmium in milk and dairy products. *Environ. Heal. Eng. Manag., vol. 10, no. 2, pp. 191–196*, https://doi.org/10.34172/EHEM.2023.21

M. S. Salman, H. Znad, M. N. Hasan, and M. M. Hasan. (2021). Optimization of innovative composite sensor for Pb(II) detection and capturing from water samples. *Microchem. J., vol. 160, no. November*, https://doi.org/10.1016/j.microc.2020.105765

N. M. Okasha and F. A. Newagy. (2024). Car-to-Car Communication Using RF Cognitive Radio With VLC Common Control Channel. *IEEE Access, vol. 12, no. May, pp. 89339–89352*, https://doi.org/10.1109/ACCESS.2024.3419072

O. Alkhazragi et al. (2023). Toward Wide-Field-of-View and Large Area Optical Detectors for High-Speed Optical Wireless Communication. *IEEE Commun. Mag., vol. 61, no. 12, pp. 162–167*, https://doi.org/10.1109/MCOM.001.2200804

O. Gholipour, N. Rajabi, M. H. Razeghi, and S. Arabi. (2025). A potentiometric sensor for highly selective and sensitive determination of lead(II) in industrial effluents using a synthesized metal organic framework based on zinc(II) and 4-methyl-1,2,4-triazole-3-thiol: Density functional theory and experimental study. *Microchem. J., vol. 212, no. January*, https://doi.org/10.1016/j.microc.2025.113496

P. Sharda, G. S. Reddy, M. R. Bhatnagar, and Z. Ghassemlooy. (2022). A Comprehensive Modeling of Vehicle-to-Vehicle Based VLC System Under Practical Considerations, an Investigation of Performance, and Diversity Property. *IEEE Trans. Commun., vol. 70, no. 5, pp. 3320–3332*, https://doi.org/10.1109/TCOMM.2022.3158325

P. Sikder, M. T. Rahman, and A. S. M. Bakibillah. (2025). Advancements and Challenges of Visible Light Communication in Intelligent Transportation Systems: A Comprehensive Review. *Photonics, vol. 12, no. 3*, https://doi.org/10.3390/photonics12030225

S. Cheng et al. (2023). Efficient removal of heavy metals from aqueous solutions by Mg/Fe bimetallic oxide-modified biochar: Experiments and DFT investigations. *J. Clean. Prod., vol. 403, no. September 2022, p. 136821*, https://doi.org/10.1016/j.jclepro.2023.136821

S. M. T. Haloho et al. (2022). Optimization of Nanofiber-IIPs-Pb(II) Synthesis Based on Ion Imprinted Polymers Smart Material Pb(II) Adsorbent through Voltage Variation Using Electrospinning Method. Universitas Sriwijaya. https://repository.unsri.ac.id/150541/

S. P. Najda et al. (2022). GaN Laser Diode Technology for Visible-Light Communications. *Electron., vol. 11, no. 9*, https://doi.org/10.3390/electronics11091430

S. U. Rehman, S. Ullah, P. H. J. Chong, S. Yongchareon, and D. Komosny. (2019). Visible light communication: A system perspective—Overview and challenges. *Sensors (Switzerland), vol. 19, no. 5, pp. 1–22*, https://doi.org/10.3390/s19051153

T. Yu, W. Huang, W. Lee, C. Chow, S. Chang, and H. Kuo. (2021). Visible Light Communication System Technology Review: Devices, Architecture, and Applications. *crystals, vol. 1098, no. 11*, doi: https://doi.org/10.3390/cryst11091098.

V. Kavitha, B. A. Vijayalakshmi, and M. Vanitalakshmi. (2024). VLC-based DCO-OFDM and WSN in hospitals for medical information transmission. *J. Opt., vol. 53, pp. 4988–4996*. https://doi.org/10.1007/s12596-024-01729-w

W. C. Wang, H. Y. Wang, and G. R. Lin. (2018). Ultrahigh-speed violet laser diode based free-space optical communication beyond 25 Gbit/s. *Sci. Rep., vol. 8, no. 1, pp. 4–10*, https://doi.org/10.1038/s41598-018-31431-4

WHO (2022). Guidelines for drinking-water quality: fourth edition incorporating the first and second addenda. *World Health Organization*, ISBN 978-92-4-004506-4.

W. Wu et al. (2022). Hydroxyapatite tailored hierarchical porous biochar composite immobilized Cd(II) and Pb(II) and mitigated their hazardous effects in contaminated water and soil. *J. Hazard. Mater., vol. 437, no. March*, https://doi.org/10.1016/j.jhazmat.2022.129330

X. Cai et.al. (2014). Novel Pb2+ Ion Imprinted Polymers Based on Ionic Interaction via Synergy of Dual Functional Monomers for Selective Solid-Phase Extraction of Pb2+ in Water Samples. *ACS APPLIED MATERIALS & INTERFACES*, 6, 305-313. https://doi.org/10.1021/am4042405

X. Zhou, B. Wang, and R. Wang. (2022). Insights into ion-imprinted materials for the recovery of metal ions: Preparation, evaluation and application. *Sep. Purif. Technol., vol. 298, no. June, p. 121469*, https://doi.org/10.1016/j.seppur.2022.121469

Y. Almadani et al. (2020). Visible light communications for industrial applications—challenges and potentials. *Electron., vol. 9, no. 12, pp. 1–38*, , https://doi.org/10.3390/electronics9122157

Y. Fan et al. (2020). Long-term continuous and real-time in situ monitoring of Pb(II) toxic contaminants in wastewater using solid-state ion selective membrane (S-ISM) Pb and pH auto-correction assembly. *J. Hazard. Mater.,* vol. 400, no. March, https://doi.org/10.1016/j.jhazmat.2020.123299

Y. Fang et al.(2024). Fluorescence detection and effective adsorption of trace Pb(II) based on nanofibrous metal-organic gel. *Chem. Synth.*, *vol. 4, no. 3*, https://doi.org/10.20517/cs.2024.06

Y. Permatasari and M. M. Sianita. (2025). Optimization of pH Conditions for Lead Adsorption using Ion- Imprinted Polymer (IIP) with EDTA as Ligand. *Indones. J. Chem. Anal., vol. 08, no. 01, pp. 31–39*, https://doi.org/10.20885/ijca.vol8.iss1.art3.

Y. Qin and Y. Tao. (2022). Pollution status of heavy metals and metalloids in Chinese lakes: Distribution, bioaccumulation and risk assessment. *Ecotoxicol. Environ. Saf.,* vol. 248, https://doi.org/10.1016/j.ecoenv.2022.114293